Impedance-Based Stability Analysis of Systems with the Dominant Presence of Distributed Power Sources

Kazuki Ohuchi[1], Yuko Hirase[1*]and Marta Molinas[2]
1 Department of Electrical, Electronic and Communications Engineering, Toyo University, Kawagoe, Japan
2 Department of Engineering Cybernetics, Norwegian University of Science and Technology, Trondheim, Norway
*E-mail: hirase028@toyo.jp

Abstract— **In recently developed electric power systems, numerous distributed generators (DGs) are connected via power electronic devices. Because these devices can generate harmonics and nonlinear distortion, traditional model-based approaches can become too complex to accurately analyze the dynamic responses of DGs. Stability analysis methods based on impedance scanning provide a practical alternative to the linear model approximation method; they directly measure the impedance of the source-load subsystems and evaluate the stability. However, most previous research focused on the characteristics of individual grid-connected devices and the stability of the microgrid (MG). In this study, the dynamic characteristics of a large-scale power system with intermittencies caused by the introduction of a large number of DGs with advanced inverter controls were analyzed through impedance-based analysis. The effect of the capacitance of passive filters and transmission lines in advanced DGs on stability was also investigated.**

Keywords— advanced inverter, impedance, stability, transient responses

I. INTRODUCTION

Recently, to maintain sustainable and stable use of energy, the electric power system has been configured as a set of microgrids (MGs) that are mainly composed of various types of distributed generators (DGs) instead of centralized power plants. For the DGs to be connected to the power system, power electronic devices, such as rectifiers and inverters, with various sophisticated functions are required. However, because these devices can generate many harmonics and can lead to nonlinear distortion, numerous DGs may lead to the instability of the entire system [1]. This issue is prominent for autonomous systems in isolated MGs and may have adverse effects on load operations such as induction motors. Therefore, to stably operate a power system with intermittencies caused by DGs, a practical method is required for acquiring and analyzing the dynamic characteristics of the system with high accuracy.

Conventional methods typically use a model-based approach, for example, small-signal modeling, when steady-state stability is required. Hiti et al. [2] presented the modeling of a three-phase pulse-width modulation (PWM) inverter on dq synchronous coordinates, which is the basis of model-based analysis. Although this approach is useful for small-signal model-based inverter analysis, it is insufficient for analyzing systems in which inverters equipped with various types of controls are connected to complex power systems at arbitrary instants. A practical alternative to model-based analysis for these complex systems is the impedance-based analysis method, which measures the source-load impedance at the target area and evaluates its stability. Belkhayat [3] introduced various load models and confirmed the consistency between the results of impedance-based analysis and mathematical models. An overview of small-signal stability analysis methods and the practical advantages of impedance-based analysis is presented in [4] and [5]. Methods that reduce the computational load of numerical analysis in impedance-based methods have also been introduced [6,7]. With the recent increasing development of measurement and communication technologies, research on impedance-based analysis as data-driven analysis has accelerated, and analysis results from demonstration machine tests have been published [8,9]. Wen et al. [10−13] performed impedance-based analysis on an inverter-based MG and published numerous relevant findings. Amin et al. [14,15] extended the inverter-based MG and performed eigenvalue analysis using high-voltage direct current (HVDC) transmission systems as an example. Rygg et al. [16−18] applied impedance-based analysis in the dq domain to the positive/negative sequence domain and proved that analyses in both domains were equivalent. In [19], an impedance-based analysis was performed on an MG consisting of two types of advanced controlled inverters (grid-forming type and grid-following type).

Thus, most previous research has focused on MG stability based on the characteristics of grid-connected inverters or loads. For example, a multi-converter study based on impedance analysis investigated the impact of connecting a new inverter at different points in the system, which can be useful in expansion-planning studies [20]. In contrast, this study assumed that numerous DGs are connected to a distribution system with a power plant comprising conventional synchronous generators (SGs). To reflect the current widespread

adoption of renewable in a move toward carbon neutrality, this study analyzes the effect of DGs connected to a low-voltage distribution system at a long distance from the plant. In particular, assuming a situation in which the generation ratio of DGs becomes dominant compared to that of SGs in the future, the effects of the capacitance of transmission and distribution lines and the passive filter capacitance of grid-connected inverters will be discussed.

II. METHODOLOGY

A. Theory of impedance-based stability

The algorithm used in this study is briefly reviewed, and its detailed derivation is provided in [18]. A general power system can consist of two subsystems (i.e., a source and a load) connected via an appropriate interface point, namely, the point of common coupling (PCC). The source subsystem is represented by a Thévenin equivalent circuit with equivalent impedance Z_S . The load subsystem is represented by a Norton equivalent circuit with equivalent load admittance $Y_L = Z_L^{-1}$. A DC system can be analyzed using the Nyquist criterion by defining the minor-loop gain as follows: $L(s) = Z_S Y_L$ [21]. However, owing to its simplicity, the three-phase AC system on the stationary frame is typically converted to the dq reference frame. In this case, the system is a multi-input multi-output (MIMO) system, to which the generalized Nyquist criterion (GNC) can be applied. The GNC is an extension of the classical Nyquist criteria derived for single-input single-output (SISO) systems, such as DC systems. Following the modified GNC explained in [3] and [18], system stability can be assessed by the condition that all eigenvalue loci of the minor-loop gain $L(s)$ do not encircle the point $(-1, j0)$. The eigenvalue of $L(s)$ can be calculated from (1), where $\lambda_i(s)$ is the i -th eigenvalue of $L(s)$.

$$\det\left(I + L(s)\right) = \prod_i \left(1 + \lambda_i(s)\right). \tag{1}$$

Fig. 1 shows the system configuration and the block diagram of an AC system. Here, s represents the Laplace operator, and the superscript dq indicates that each variable is defined in the dq domain by disregarding the zero-sequence component. The small-signal source impedance $\boldsymbol{Z}_s^{dq}(s)$ and load admittance $\boldsymbol{Y}_L^{dq}(s)$ can be calculated from (2) and (3) (the generalized Ohm's law), respectively:

$$\begin{aligned}&\boldsymbol{V}_S^{dq}(s) = \boldsymbol{Z}_S^{dq}(s)\boldsymbol{I}_S^{dq}(s)\\ &\Leftrightarrow \begin{bmatrix} V_S^d(s) \\ V_S^q(s) \end{bmatrix} = \begin{bmatrix} Z_S^{dd}(s) & Z_S^{dq}(s) \\ Z_S^{qd}(s) & Z_S^{qq}(s) \end{bmatrix} \begin{bmatrix} I_S^d(s) \\ I_S^q(s) \end{bmatrix},\end{aligned} \tag{2}$$

$$\begin{aligned}&\boldsymbol{I}_L^{dq}(s) = \boldsymbol{Y}_L^{dq}(s)\boldsymbol{V}_L^{dq}(s)\\ &\Leftrightarrow \begin{bmatrix} I_L^d(s) \\ I_L^q(s) \end{bmatrix} = \begin{bmatrix} Z_L^{dd}(s) & Z_L^{dq}(s) \\ Z_L^{qd}(s) & Z_L^{qq}(s) \end{bmatrix} \begin{bmatrix} V_L^d(s) \\ V_L^q(s) \end{bmatrix}.\end{aligned} \tag{3}$$

The small-signal impedance of the three-phase AC systems is calculated by measuring the response to a small disturbance in the simulation. The small disturbances can be caused by signal injection through frequency sweeping at the PCC using two types of methods: series voltage or shunt current injection. In this study, DGs with a large output ratio were set as the source side, and the conventional SGs were set as the load side. To reduce the measurement error, two orthogonal signals were injected at the connection point of the output filter of the DGs in the series voltage method [16].

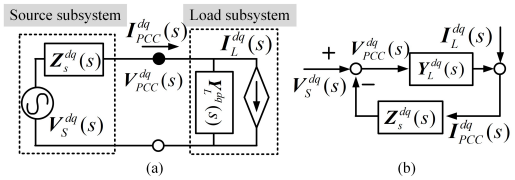

Fig. 1. AC system in the dq domain: (a) system configuration and (b) block diagram.

B. Advanced inverter (VSG) control

DGs derived from renewables, such as photovoltaic power generation, threaten the stability of power systems due to their intermittency, which depends on weather conditions and the nonlinearity of harmonics generated by power electronic devices. Furthermore, power electronic devices do not have the inertia of traditional SGs and introducing large amounts of DGs reduces the inertia of the entire grid. Therefore, inverters that interconnect these DGs to the grid are expected to have functions that contribute to stabilizing the frequency and voltage. Unlike grid-following inverters such as those in conventional power conditioning systems, some grid-forming inverters have a control mechanism that simulates the inertial behavior, similar to that of SGs, thereby becoming the main power source themselves or promoting grid stability.

Virtual synchronous generator (VSG) control is an advanced control of grid-connected inverters that can output power equivalent to the inertial energy based on Park's generator theory; the control uses stored energy such as batteries or super capacitors connected at the DC side of the inverter. The above mentioned virtual-inertial behavior, like that of SGs, has a frequency response in the 0.1 Hz to several Hz band, whereas the cutoff frequency of the passive output filter of the inverter is designed to be approximately 1 kHz to several kHz for conventional Si IGBTs. These output filters have capacitance components to enable islanded operation of a grid-forming inverter. In addition, VSG control has a cross-coupled term between the excitation and torque controls. Considering these factors, the output behavior must be analyzed in all frequency bands when a large number of DGs with advanced control such as VSG is introduced into the grid via inverters.

Although various types of VSG controls have been studied, they all have been introduced with the motivation of simulating the inertial control of a synchronous generator. Therefore, in this study, Kawasaki-type VSG control [22], which can be easily

constructed as a power control at the supervisory layer of a conventional grid-following inverter, is verified. From this point, DGs of grid-connecting inverters with Kawasaki inverter control will be referred to as VSGs.

Fig. 2 shows the Kawasaki topology used for VSG control, which consists of torque control, excitation control, and the impedance model shown in the red, blue, and green frames, respectively. The current command values are calculated and output to the minor control, which is conventional current control. In torque control, the internal phase difference angle (δ rad) is calculated from the difference between the command and feedback values of the active power (P pu and P^* pu) and the difference between the angular velocity of the inverter output voltage (ω rad/s) and its nominal value (ω_n rad/s). The angular velocity difference has a droop characteristic of K_{PF} with respect to the active power difference. When this is combined with the swing equation for the inertial constant (M s), the dynamics of the torque control can be expressed as follows: $G(s)=-1/(sM+K_{PF})$. Here, s denotes the Laplace variable, and the delay time of the virtual governor can be assumed to be zero. Similarly, in the excitation control, the RMS value ($|\boldsymbol{E}_f|$ pu) of the generator voltage vector ($\boldsymbol{E}_f$) is calculated using the difference between the command and feedback values of the reactive power (Q pu and Q^* pu) and the difference between the RMS value ($|\boldsymbol{V}_g|$ pu) of the inverter voltage vector ($\boldsymbol{V}_g$) and its nominal value (1 pu). The voltage difference has a droop characteristic of K_{QV} with respect to the reactive power difference, and the dynamics, including this droop characteristic and the delay time T_m of the power measurement, is represented by $K(s)=K_{QV}/(sT_m+1)$. $|\boldsymbol{E}_f|$ is maintained at 1 pu by an automatic voltage regulator (AVR) represented by proportional-integral compensation ($H(s)$). Letting Δ denote the power variation, δ and $|\boldsymbol{E}_f|$ are expressed by (4) and (5), respectively. Here, Here, ω_n rad/s is the nominal angular velocity. Using (6), the current command value vector $\boldsymbol{I}^*=[i_d^*, i_q^*]^{\mathrm{T}}$ is calculated in the impedance model from $\boldsymbol{E}_f=[e_d, e_q]^{\mathrm{T}}$, $\boldsymbol{V}_g=[v_d, v_q]^{\mathrm{T}}$.

$$\delta=\omega_n(\Delta P\cdot G(s)/s)+(\omega_n-\omega)/s\,. \tag{4}$$

$$|\boldsymbol{E}_f|=H(s)(\Delta Q\cdot K(s)-|\boldsymbol{V}_g|)\,. \tag{5}$$

$$\boldsymbol{I}^*=\begin{bmatrix} i_d^* \\ i_q^* \end{bmatrix}=\frac{1}{r^2+x^2}\begin{bmatrix} r & x \\ -x & r \end{bmatrix}\left(\begin{bmatrix} e_d \\ e_q \end{bmatrix}-\begin{bmatrix} v_d \\ v_q \end{bmatrix}\right). \tag{6}$$

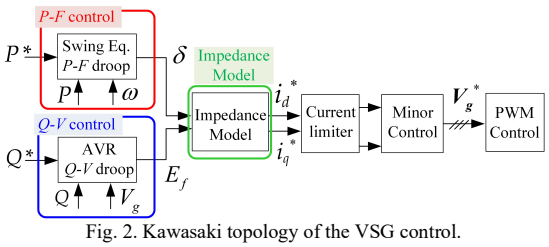

Fig. 2. Kawasaki topology of the VSG control.

The VSG inverter simulates not only the steady-state response of an SG but also the dynamic response of it. The steady-state refers to the governor-free state, where the differential terms of the dynamic equation are expressed as zero and is determined by K_{PF} . In contrast, the dynamic inertial response, which is usually in ~0.1−10 Hz, is determined by M . The virtual resistance (r) and virtual reactance (x), which cause the mutual interference between the torque control of the d-axis and excitation control of the q-axis, determine the initial transient state until the inertial response is activated. These values can also be set in the software, and in this study, they were set to $r=0.4$ pu and $x=0.2$ pu. Here, K_{PF} , M , r , and x are all software variables, and considering that their effects appear at least after one control period, the hardware should respond to disturbances the fastest in the system. The main circuit of the grid-connected inverter is the output filter, whose impedance dominates in the frequency range of ~10-20 kHz [23].

C. *Target system*

Fig. 3 shows the circuit diagram used in the simulation. PSCAD/EMTDC was used for data measurement. The constants of the main circuit are also shown in the figure. The subsystem comprises SGs and VSGs, and assuming a future power system in which power generation by DGs becomes dominant, the total capacity of the SGs was 60 MVA and that of the VSGs was 240 MVA. The energy source on the DC side of the VSGs was assumed to be supplied at a sufficiently high speed. The synchronous reactance values of SGs were $x_d=1.71$ and $x_q=1.65$ pu, and the transient reactance values were $x_d'=0.23$ and $x_q'=0.37$ pu. Each SG had the same control, including a thermal and nuclear plant governor system model (LPT = 1), and a thyristor excitation model equipped with a ΔP-type power system stabilizer (PSS) (LAT =102) [22]. The set points of both generators for the base load were set to maintain each terminal voltage and frequency at the rated values (SGs: 18 kV and 50 Hz; DGs: 0.4 kV and 50 Hz). The transmission line from the perturbation injection point to the SG was divided into three π -type sections ($\pi 1$, $\pi 2$, and $\pi 3$) by the transformers and base load. The resistance, impedance, and admittance of each section were approximately $r=0.047$ Ω/km, $x=0.348$ Ω/km , and $y=3.3$ μS/km , respectively. Signal perturbation started at the steady-state condition with a base load of 100 MW. The amplitude of the perturbation

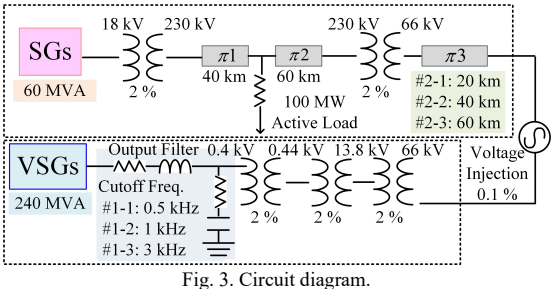

Fig. 3. Circuit diagram.

signals was set to 0.1 % of 66 kV. The frequency of the perturbation signal was swept in the range of 1 Hz to 15 kHz, and the currents and voltages were measured at 51 different frequencies. The simulation time step was set to 20 μs .

The effects of the differences in control logic and parameters within each subsystem are not investigated in this study; hence, they should be investigated in the future. This study reports the test results of the following two types of tests:

- In test #1: the inductance of the passive output filter in VSGs was kept constant, and the capacitance was varied. In #1-1, #1-2, and #1-3, the cutoff frequencies of the VSGs were 0.5 kHz, 1 kHz, and: 3 kHz, respectively. In this case, the length of $\pi 3$ was set to 20 km.
- In test #2: the stabilities of varying $\pi 3$ lengths were compared (#2-1: 20 km, #2-2: 40 km, and #2-3: 60 km). The cutoff frequency of the VSGs was 1 kHz. Tests #1-2 and #2-1 were the same.

III. Results of the Impedance-Based Analysis

A. *Tests varying the cutoff frequency of the VSGs*

Figs. 4(a) and 4(b) show the output impedance of the

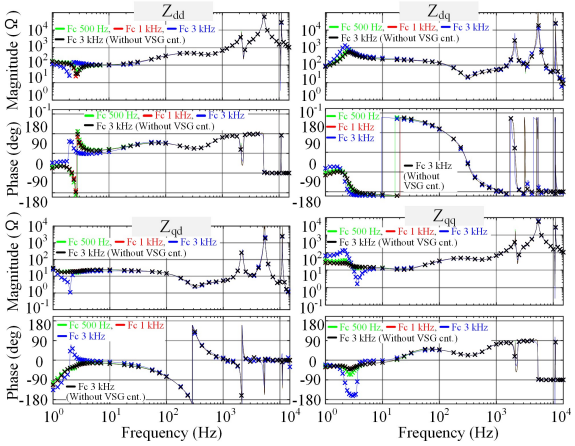

(a) Output impedance of SGs ($\boldsymbol{Z}_{SG}$).

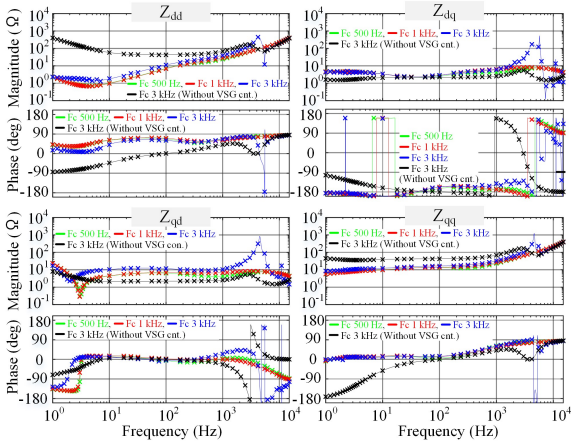

(b) Output impedance of VSGs ($\boldsymbol{Z}_{VSG}$).

Fig. 4. Output impedance of subcircuits in test #1.

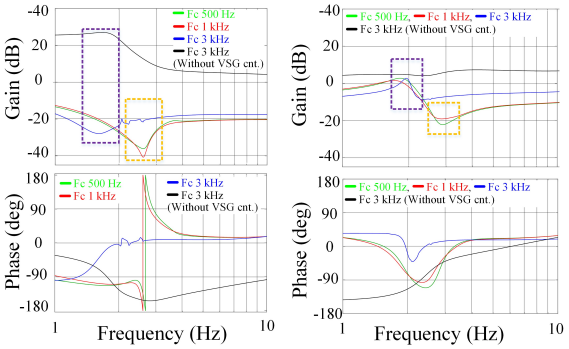

(a) Bode plots in 1−10 Hz: λ_1 (left) and λ_2 (right).

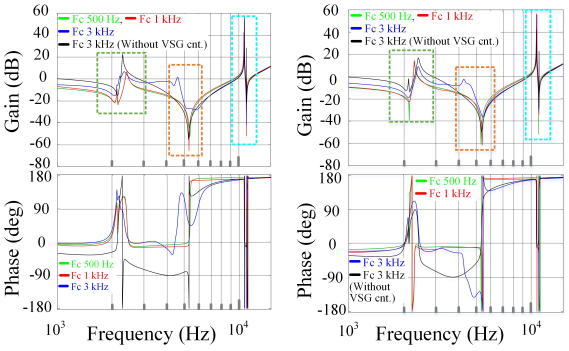

(b) Bode plots in 1−20 kHz: λ_1 (left) and λ_2 (right).

Fig. 5. Bode plots of the eigenvalues of the minor-loop gain in test #1.

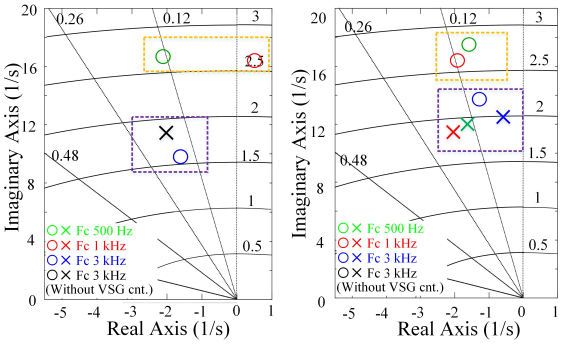

(a) Pole/zero plots in 1−3 Hz: λ_1 (left) and λ_2 (right).

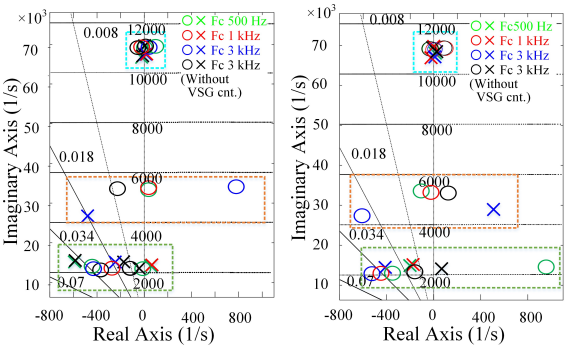

(b) Pole/zero plots in 2−12 kHz: λ_1 (left) and λ_2 (right).

Fig. 6. Pole/zero plots of the eigenvalues of the minor-loop gain in test #1.

SGs ($\boldsymbol{Z}_{SG}$) and VSGs ($\boldsymbol{Z}_{VSG}$), respectively, calculated from the results of tests #1-1, #1-2, and #1-3, in which the cutoff frequency of the VSGs was varied. The green, red, and blue lines in Fig. 4 represent the impedance characteristics when the cutoff frequencies were 0.5 kHz (#1-1), 1 kHz (#1-2), and 3 kHz (#1-3), respectively. For comparison, the impedance was superimposed in black when the VSG control in the upper control (framed in red, blue, and green in Fig. 3) was disabled and only minor current control was used. The cutoff frequency of the output filter for this grid-following type control was set to 3 kHz. Changing the filter capacitance of the VSGs mostly led to differences in the impedance characteristics of $\boldsymbol{Z}_{VSG}$ for the different tests (Fig. 4(b)) at ~2−3 Hz and ~4−5 kHz. Considering that the gain peak disappears when the cutoff frequency of the filter is reduced or the VSG control is disabled, this can be attributed to the resonance between the filter capacitance with the VSG control. In contrast, $\boldsymbol{Z}_{SG}$ (Fig. 4(a)) also shows a difference in the filter capacitances at ~2−3 Hz, and there is no difference at ~4−5 kHz. These results suggest that the VSG control causes resonance between it and SG control in the low frequency band, and the filter

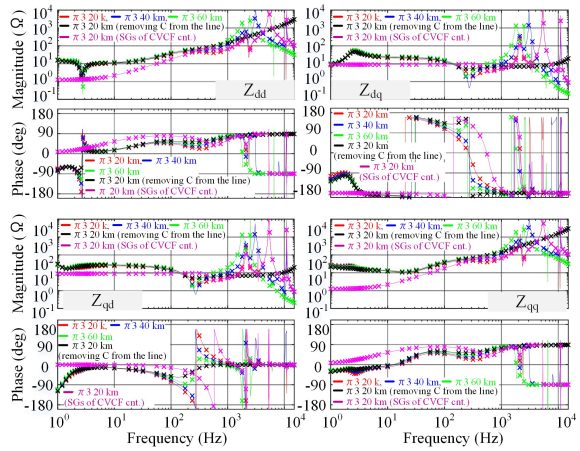

(a) Output impedance of SGs ($\boldsymbol{Z}_{SG}$).

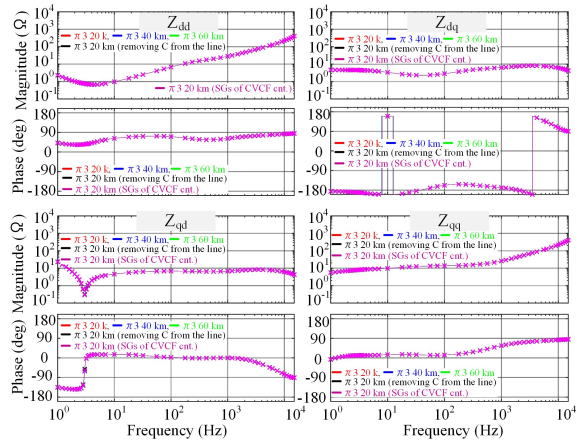

(b) Output impedance of VSGs ($\boldsymbol{Z}_{VSG}$).

Fig. 7. Output impedance of subcircuits in test #2.

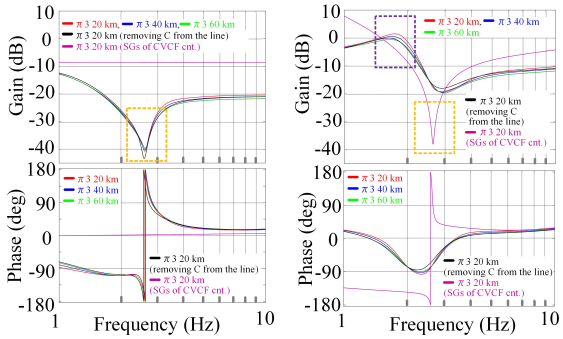

(a) Bode plots in 1−10 Hz: λ_1 (left) and λ_2 (right).

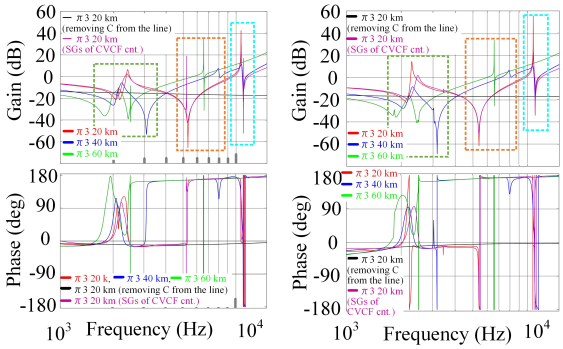

(b) Bode plots in 1−20 kHz: λ_1 (left) and λ_2 (right).

Fig. 8. Bode plots of the eigenvalues of the minor-loop gain in test #2.

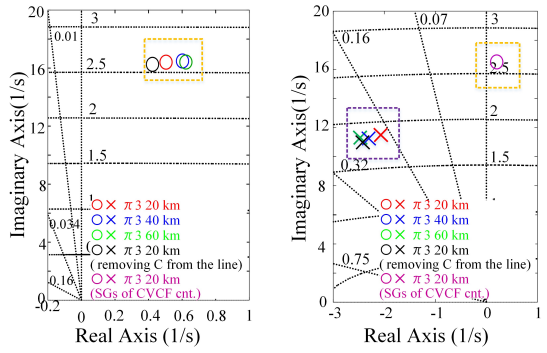

(a) Pole/zero plots in 1−3 Hz: λ_1 (left) and λ_2 (right).

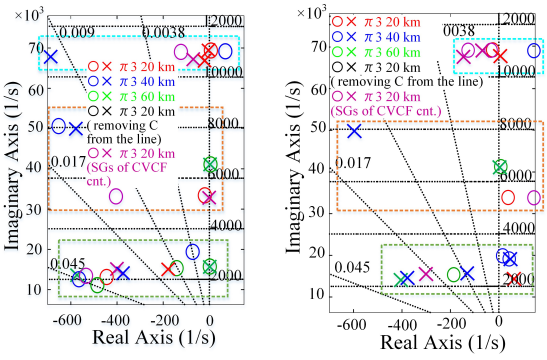

(b) Pole/zero plots in 2−12 kHz: λ_1 (left) and λ_2 (right).

Fig. 9. Pole/zero plots of the eigenvalues of the minor-loop gain in test #2.

capacitance can be dominant in the high frequency band.

Figs. 5 and 6 show the bode and pole/zero plots of the two eigenvalues (λ_1 and λ_2) of the minor-loop gain in test #1, respectively. The non-dominant poles and zeros were manually canceled. Fig. 5(a) and Fig. 6(a) show the characteristics in the low frequency range, and Figs. 5(b) and 6(b) showed them in the high frequency range. Unstable poles around 4.5 kHz (blue) and 2.1 kHz (black) are clearly visible for the same cutoff frequency of 3 kHz. On the other hand, the test results with a lower cutoff frequency (red and green) show no unstable poles. These features are similar to those in Fig. 4(b), indicating that the unstable poles are due to resonance between the output filter and control. It can also be considered that the VSG control moved the unstable poles to the high frequency band.

B. Tests varying the length of the π section

Fig. 7 shows the characteristics of the output impedance calculated from the results of tests #2-1, #2-2, and #2-3. Fig. 7(a) shows the impedance of the SGs ($\boldsymbol{Z}_{SG}$), and Fig. 7(b) shows that of the VSGs ($\boldsymbol{Z}_{VSG}$). The red, blue, and green lines represent the impedance characteristics when the transmission line lengths were 20 km (#2-1), 40 km (#2-2), and 60 km (#2-3), respectively. For comparison, the result for all the transmission lines with no capacitance is depicted in black, and the result of running SGs in constant voltage and constant frequency modes is shown in magenta. Because the $\pi 3$ section was located at the SG side from the perturbation point, a significant difference due to the length of $\pi 3$ is observed in $\boldsymbol{Z}_{SG}$ (Fig. 7(a)). As shown in Fig. 4(a), the significant gain peaks in the high frequency band of 1−15 kHz must be independent of the VSGs. Furthermore, because disabling the inertial control of SGs and removing the capacitance

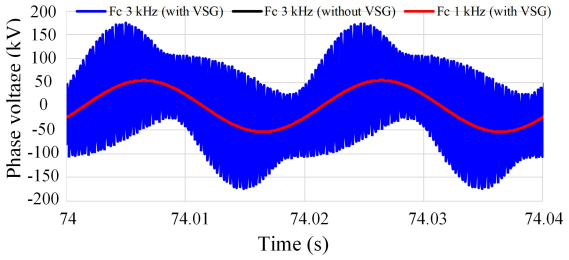

(a) AC voltage (u-phase).

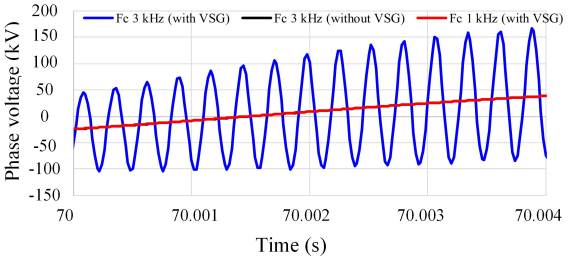

(b) Enlarged u-phase voltage of (a).

Fig. 10. AC voltage (u-phase) when the cutoff frequency of the output filter was set to 3 kHz.

in $\pi 3$ could not and could eliminate the resonances, respectively, the above frequencies must be natural frequencies in $\pi 3$ and the resonances occurred within the π -section.

Figs. 8 and 9 show the bode and pole-zero plots of the two eigenvalues (λ_1 and λ_2) of the minor-loop gain in test #2, respectively. Figs. 8(a) and 9(a) indicate the characteristics in the low frequency range, whereas Figs. 8(b) and 9(b) show the characteristics in the high frequency range. Similar to test #1, the natural oscillations of the π -section observed in Fig. 7(a) are also evident in the characteristics of the minor-loop gain.

Generally, to study the eigenvalues of power systems, every 5−10 km of the line length must be modeled in a single π -section [24]. In this study, to avoid complicating the analysis results, the transmission line of the target circuit was divided into three π -sections, and the length of $\pi 3$ was varied between 20 and 60 km. Including the discussion regarding the modeling accuracy, impedance analyses by changing the number of sections and length of one section need to be addressed.

IV. Results of the Time-Domain Simulation

A. Tests when the cutoff frequency was 3 kHz

Fig. 10 shows the AC voltage at a steady state when the length of $\pi 3$ was 20 km. Fig. 10(a) shows the u-phase of the AC voltage, and Fig. 10(b) shows the enlarged voltage of Fig. 10(a). The black and blue line show the results without and with VSG controls, respectively, when the cutoff frequency was 3 kHz. The red line shows the result with VSG control and a cutoff frequency of 1 kHz, and the black and red lines overlap. The oscillation frequency of 4.5 kHz in the blue line exactly matches the results obtained from the impedance analyses (Fig. 4). As discussed in the previous section, voltage oscillation can be avoided by changing the value of the filter capacitance to reduce the cutoff frequency or by disabling the VSG control of the DGs even at the same cutoff frequency. The loop gains of the VSG and minor-current controls may be the cause of the unstable resonance and is currently under investigation.

B. Tests when the additional DG was connected

The impedance analysis in the previous section showed that the $\pi 3$ section had natural frequencies around 1−15 kHz. If the grid-connected inverter connected to this π -section contains harmonics in this frequency band, resonance among the inverter and π -section is expected. Therefore, to confirm the time response of this resonance, an additional DG was connected to the $\pi 3$ section. The DG was connected via a grid-following-type inverter and was expected to generate 8 MW of power. We planned three cases in which the generated power contained 23 % harmonics at 1, 2, and 5 kHz. Figs. 11 and 12 show the steady-state AC voltages and currents when an additional DG was connected, respectively. The green, blue, and red lines represent the results measured when the injected

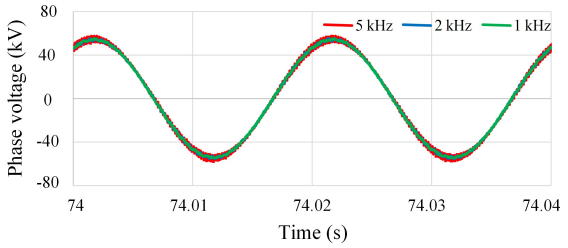

(a) AC voltage.

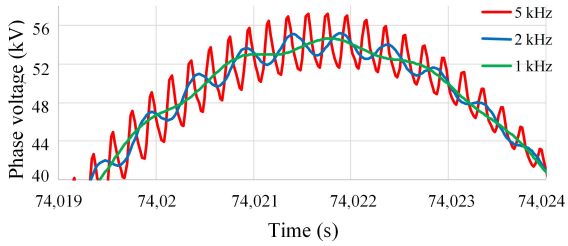

(b) Enlarged AC voltage of (a).

Fig. 11. AC voltage when the additional DG with harmonics was connected.

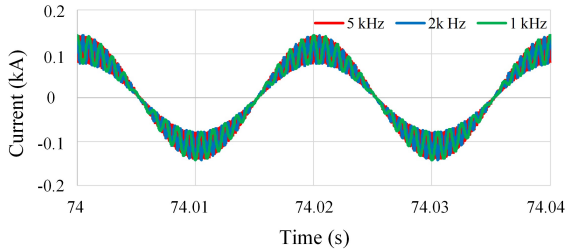

(a) AC current.

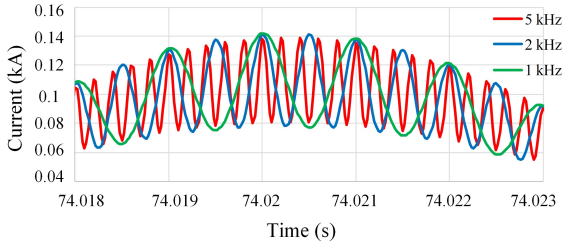

(b) Enlarged AC current of (a).

Fig. 12. AC current when the additional DG with harmonics was connected.

harmonic components were 1, 2, and 5 kHz, respectively. The harmonic currents generated by the additional DG (Fig. 12) also affected the grid voltages (Fig. 11). Even when all the harmonic currents were set to 23 %, the 2 kHz and 5 kHz harmonic voltages were more noticeable than the 1 kHz harmonic voltage. This is consistent with the results of impedance analysis in the previous section.

From the results and analysis presented in this paper, it is clear that impedance analysis will be a very valuable tool for grid operators to identify the intrinsic frequencies of transmission lines and other equipment. Also, manufacturers of grid-connected inverters will strongly benefit from the use of impedance analysis when designing PWM circuits to avoid these resonance frequencies. Altogether this will contribute to the stable operation of the grid.

V. Conclusion

In this study, the stability of power systems with DGs was evaluated by changing the transmission line length and the cutoff frequency of the output filter of grid-connected inverters with the assumption that DGs dominate the power system. When all DGs are connected by advanced inverters, the filter capacitance contained in the grid-connected inverter of the DGs of the dominant generation output and non-negligible capacitance in the long transmission lines cause unstable oscillation in the voltage of the system. VSG control, which simulates the inertia of SGs, has been actively used in interconnected inverters because it contributes to the transient stabilization of the grid. Although the VSG control can be easily added to the supervisory layer of current control of grid-following inverters, it can change the resonant frequency between the hardware and control. Therefore, impedance analysis is useful for studying the natural frequencies in advance by considering the existing hardware and software information in detail.

Sensitivity analysis by changing the control parameters and improving the stability margins of the output impedance remain as topics for further research. Furthermore, to validate these results, mathematical analysis and additional test cases in the time-domain simulations are required.

VI. Acknowledgement

The authors would like to acknowledge the open access publication support to the project “NTNU-Chinese Collaboration on Next Generation Power Electronics Converters for Renewable Energy (CoNeCt)” 309253 funded by the Research Council of Norway under the INTPART programme.

References

[1] K. Sakimoto, Y. Miura, and T. Ise, “Stabilization of a power system with a distributed generator by a virtual synchronous generator function,” in *Proceedings of IEEE Power Electronics and ECCE Asia (ICPE & ECCE)*, Jeju, Korea, 2011, pp. 1498-1505.

[2] S. Hiti, D. Boroyevich, and C. Cuadros, “Small-signal modeling and control of three-phase PWM converters,” in *Proceedings of 1994 IEEE Industry Applications Society Annual Meeting*, 1994, pp. 1143-1150.

[3] M. Belkhayat, “Stability criteria for AC power systems with regulated loads,” Ph.D. dissertation, Purdue Univ., West Lafayette, IN, US, 1997.

[4] J. Sun, “AC power electronic systems: Stability and power quality,” in *2008 11th Workshop on Control and Modeling for Power Electronics*, Zurich, Switzerland, 2008.

[5] J. Sun, “Small-signal methods for AC distributed power systems–a review,” *IEEE Trans. on Power Electronics*, vol. 24, no. 11, pp. 2545-2554, 2009.

[6] H. Mao, D. Boroyevich, and F. C. Lee, “Novel reduced-order small-signal model of a three-phase PWM rectifier and its application in control design and system analysis,” *IEEE Transactions on Power Electronics*, vol. 13, no. 3, pp. 511-521, 1998.

[7] L. Harnefors, M. Bongiorno, and S. Lundberg, "Input-admittance calculation and shaping for controlled voltage-source converters," *IEEE Transactions on Industrial Electronics*, vol. 54, no. 6, pp. 3323-3334, 2007.

[8] G. Francis, R. Burgos, D. Boroyevich, F. Wang, and K. Karimi, "An algorithm and implementation system for measuring impedance in the DQ domain," in *2011 IEEE Energy Conversion Congress and Exposition*, 2011, pp. 3221-3228,

[9] J. Sun, "Impedance-based stability criterion for grid-connected inverters," *IEEE Transactions on Power Electronics*, vol. 26, no. 11, pp. 3075-3078, 2011.

[10] B. Wen, D. Boroyevich, P. Mattavelli, Z. Shen, and R. Burgos, "Experimental verification of the generalized Nyquist stability criterion for balanced three-phase AC systems in the presence of constant power loads," in *2012 IEEE Energy Conversion Congress and Exposition (ECCE)*, 2012, pp. 3926-3933.

[11] B. Wen, D. Boroyevich, P. Mattavelli, Z. Shen, and R. Burgos, "Influence of phase-locked loop on input admittance of three-phase voltage-source converters," in *2013 Twenty-Eighth Annual IEEE Applied Power Electronics Conference and Exposition (APEC)*, 2013, pp. 897-904.

[12] B. Wen, D. Boroyevich, R. Burgos, P. Mattavelli, and Z. Shen, "Small-signal stability analysis of three-phase AC systems in the presence of constant power loads based on measured dq frame impedances," *IEEE Transactions on Power Electronics*, vol. 30, no. 10, pp. 5952-5963, 2014.

[13] B. Wen, D. Boroyevich, R. Burgos, P. Mattavelli, and Z. Shen, "Analysis of DQ small-signal impedance of grid-tied inverters," *IEEE Transactions on Power Electronics*, vol. 31, no. 1, pp. 675-687, 2015.

[14] M. Amin and M. Molinas, "Self-synchronisation of wind farm in MMC-based HVDC system," in *2016 IEEE Electrical Power and Energy Conference (EPEC)*, 2016, pp. 1-6.

[15] M. Amin and M. Molinas, "Small-signal stability assessment of power electronics-based power systems: A discussion of impedance-and eigenvalue-based methods," *IEEE Transactions on Industry Applications*, vol. 53, no. 5, pp. 5014-5030, 2017.

[16] A. Rygg, M. Molinas, E. Unamuno, C. Zhang, and X. Cai, "A simple method for shifting local dq impedance models to a global reference frame for stability analysis," *arXiv preprint arXiv:1706.08313*, 2017.

[17] A. Rygg, M. Molinas, C. Zhang, and X. Cai, "On the equivalence and impact on stability of impedance modeling of power electronic converters in different domains," *IEEE Journal of Emerging and Selected Topics in Power Electronics*, vol. 5, no. 4, pp. 1444-1454, 2017.

[18] A. Rygg, "Impedance-based methods for small-signal analysis of systems dominated by power electronics," Ph.D. dissertation, Norwegian Univ. of Science and Technology, Trondheim, Norway, 2018.

[19] E. Unamuno, A. Rygg, M. Amin, M. Molinas, and J. A. Barrena, "Impedance-based stability evaluation of virtual synchronous machine implementations in converter controllers," in *2018 International Power Electronics Conference (IPEC-Niigata 2018-ECCE Asia)*, 2018, pp. 759- 766.

[20] A. Firdaus and M. Molinas, "Design and expansion planning of parallel inverter based AC microgrids - An approach for improved stability margins," *TechRxiv*, 2020.

[21] Apparatus models and their parameters. The Institute of Electrical Eng. of Japan. [Online]. Available: http://denki.iee.jp/pes/?page_id=1058 (Last accessed: Sept. 27th, 2021)

[22] Y. Hirase, K. Abe, K. Sugimoto, K. Sakimoto, H. Bevrani, and T. Ise, "A novel control approach for virtual synchronous generators to suppress frequency and voltage fluctuations in microgrids," *Applied Energy*, vol. 210, pp. 699-710, 2018.

[23] Y. Hirase, K. Abe, K. Sugimoto and Y. Shindo, "A grid-connected inverter with virtual synchronous generator model of algebraic type," *Electrical Engineering in Japan,* vol. 184, no. 4, pp. 10-21, 2013

[24] D. Jovcic, "High voltage direct current transmission: converters, systems and DC grids," *John Wiley & Sons,* 2019